Supplementary Information for Obayashi, Luna, Nagata, Martin-Marcos, Hiraishi , Singh *et al.*

Contents:

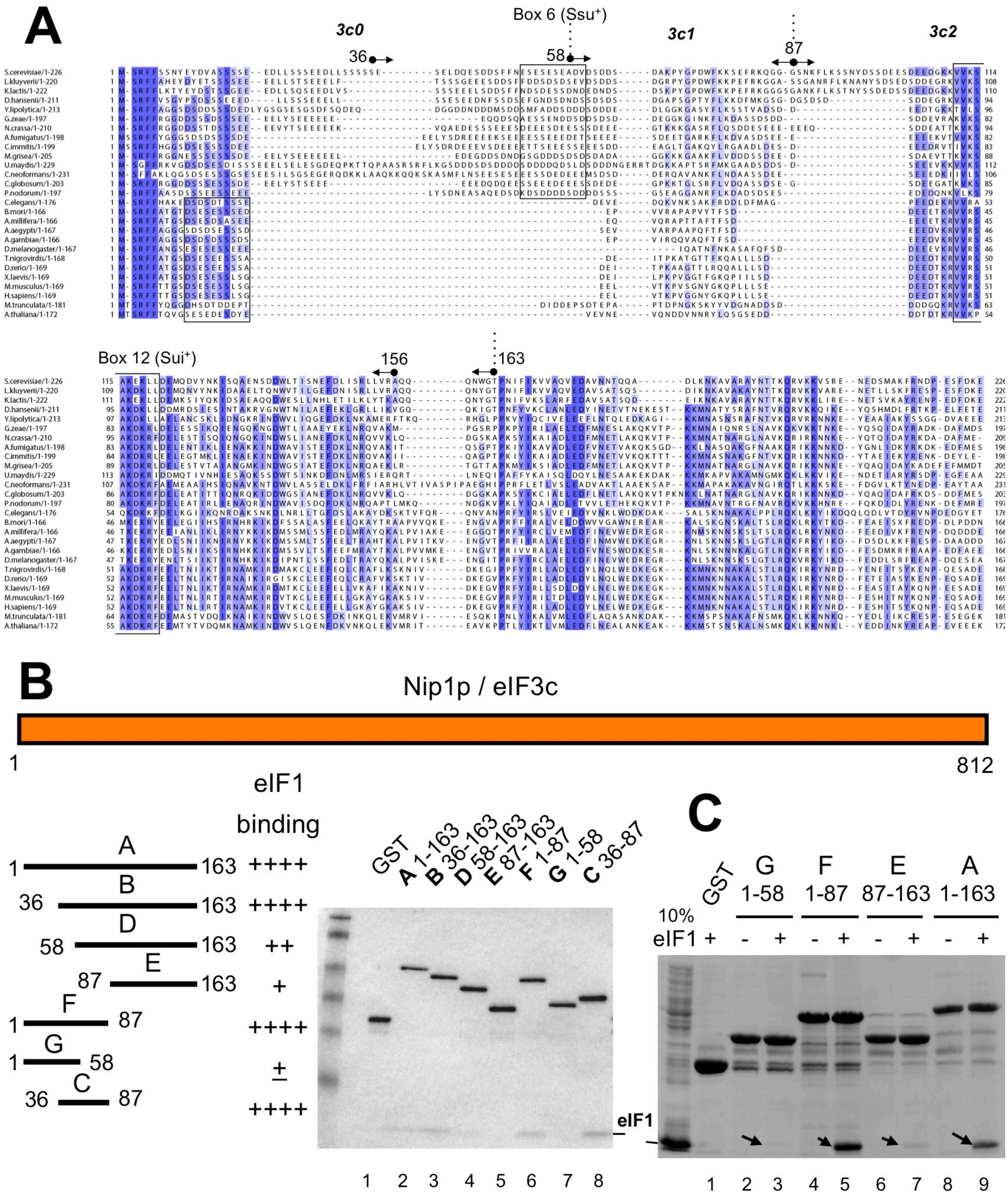

Fig. S1. Initial analysis of eIF1-binding regions in eIF3c – Related to Figure 1

(A) Alignment of eIF3c-NTD sequences from diverse eukaryotes, as generated using MUSCLE (1). Arrows indicate the location of end points for deletion constructs used in this study. Boxes indicate the location of Box6 and Box12, previously identified in yeast as the Ssu$^-$ and Sui$^-$ mutation sites. (B) and (C) GST pulldown assays. Schematic on top represents primary eIF3c structure. The lines beneath the schematic depict various truncated GST-eIF3c proteins (designated on the left). Table to the right of the schematic summarizes relative amount of eIF1 bound to the eIF3c segment fused to GST, based on all the GST pulldown experiments presented in this study. Thus, eIF3c-F and –G, which did not bind eIF1 in panel B, is shown to bind minimal amounts of eIF1 based on other GST pulldown experiments (Fig. S1C and 1B). In (B), 0.2 nmol GST fusion proteins (0.2 μM) were mixed in 1 ml binding buffer with 0.4 nmol eIF1 (0.4 μM). A fraction of the complex was isolated by glutathione sepharose chromatography and analyzed by SDS-PAGE followed by Coomassie staining. In (C), 0.12~0.17 nmol GST fusion proteins (0.6~0.9 μM) attached with the glutathione resin were mixed in 0.2 ml binding buffer with ~6 nmol eIF1 (~30 μM). After washing the resin four times, the entire pellet fractions were analyzed by SDS-PAGE and Coomassie staining.

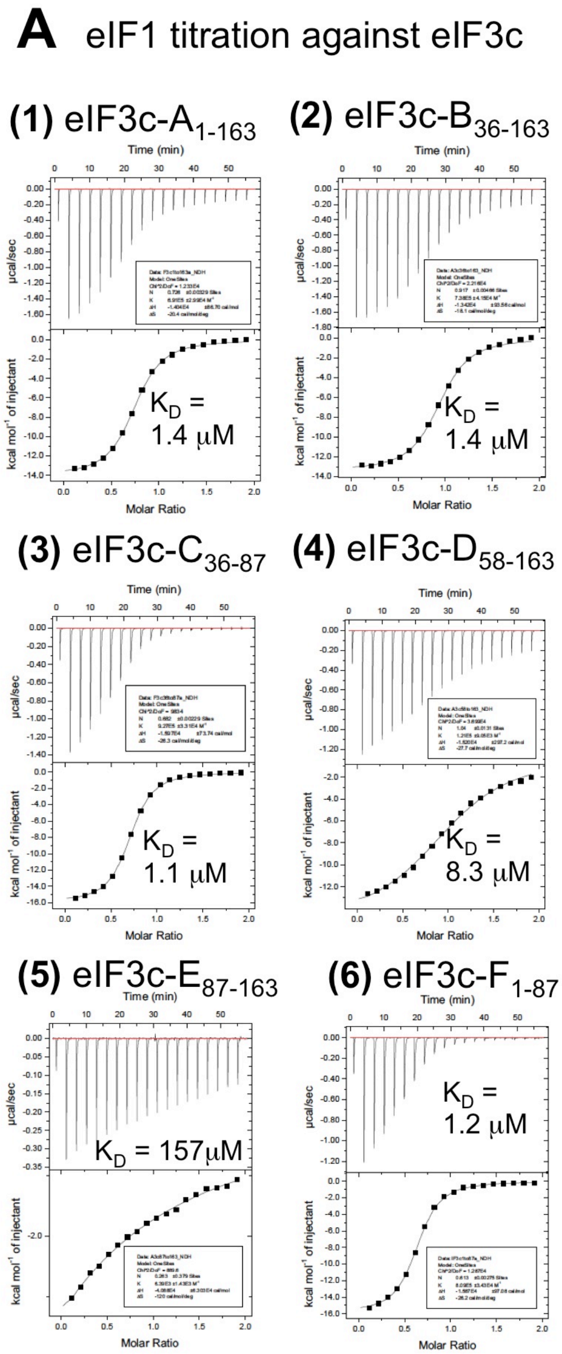

B Thermogram analysis results

Cell	Inject	*K*d (µM)	*ΔH* (kcal/mol)	*ΔS* (cal/mol/deg)	N
eIF3c-A 1-163	eIF1	1.4	-14.0	-20.4	0.72
		1.3	-13.5	-18.3	0.75
		1.5	-14.0	-20.2	0.73
eIF3c-B 36-163	eIF1	1.4	-13.4	-18.1	0.92
		1.4	-13.4	-18.1	0.95
		1.4	-13.4	-18.0	0.95
eIF3c-F 1-87	eIF1	1.2	-15.8	-25.2	0.61
		1.0	-15.9	-26.0	0.59
		0.86	-15.8	-25.5	0.55
eIF3c-C 36-87	eIF1	1.1	-16.0	-26.3	0.68
		1.2	-16.1	-26.9	0.66
		0.94	-15.8	-25.5	0.66
eIF3c-D 58-163	eIF1	8.3	-15.2	-27.7	1.04
		7.8	-14.8	-26.3	1.08
		7.8	-15.0	-27.1	1.02
eIF3c-E 87-163	eIF1	156.5	-40.9	-120	0.26
		125.9	-19.4	-47.2	0.48
		139.1	-18.0	-42.7	0.56

Fig. S2. Isothermal Titration Calorimetry (ITC) measurements. – Related to Figure 1

(A) The enthalpy changes caused by injections of eIF1 into the different fragments of eIF3c, **1)** A $_{1\text{-}163}$, 2) B $_{36\text{-}163}$, **3)** C $_{36\text{-}87}$, **4)** D $_{58\text{-}163}$, **5)** E $_{87\text{-}163}$, and **6)** GST-F$_{1\text{-}87}$. The lower panels show the fitted binding parameters; the solid line in each lower panel represents a calculated curve using the best fit parameters obtained by a nonlinear least-squares fit. (B) Summary of thermogram analysis for each of the ITC experiments (n=3) using eIF1 and the six eIF3c constructs, as shown in Fig. 1A.

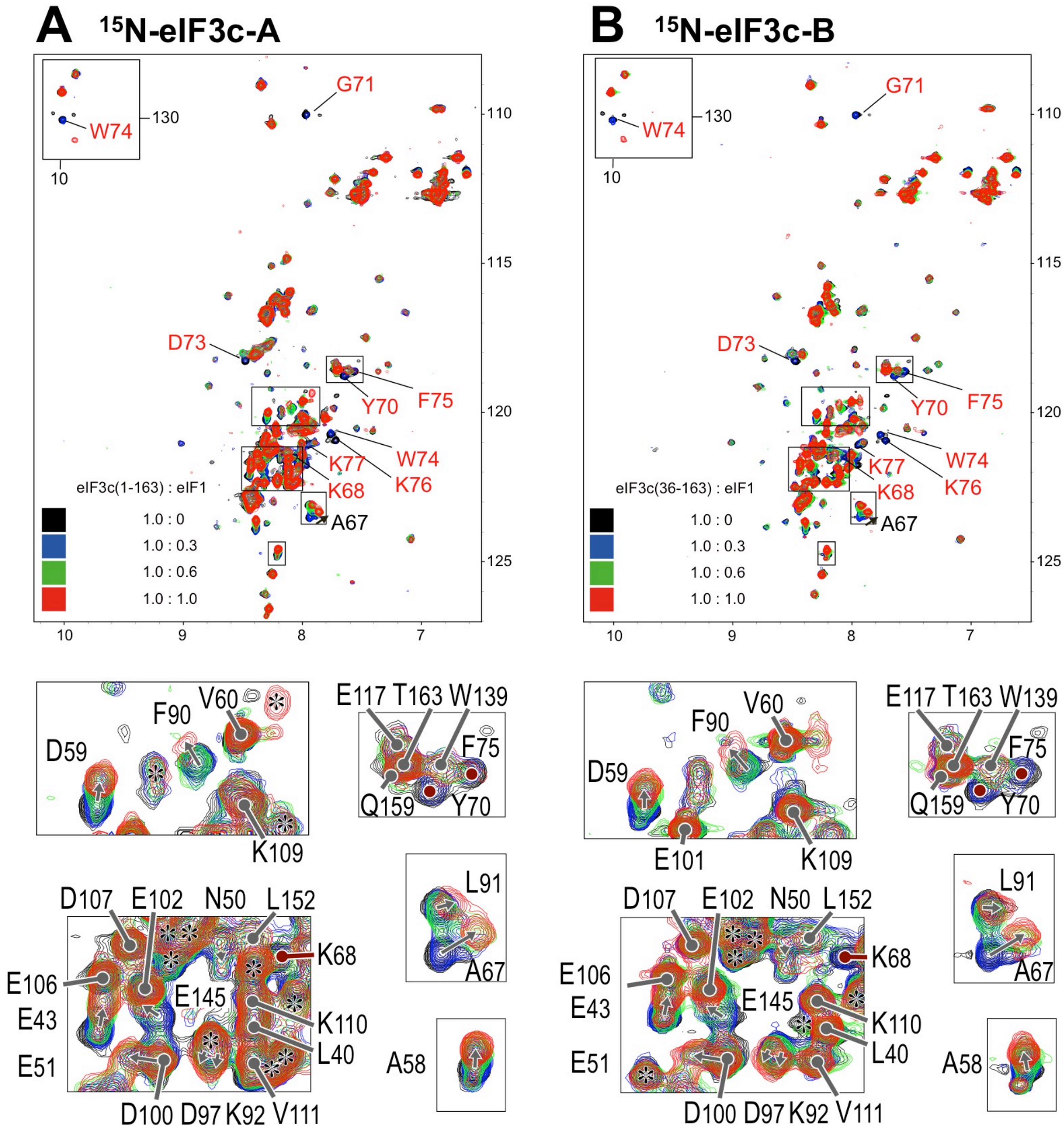

Fig. S3. CSP experiments with ^{15}N-eIF3c-A$_{1\text{-}163}$ or -B$_{36\text{-}163}$ to determine their amino acids affected by eIF1 binding. – Related to Figure 1

^{1}H-^{15}N HSQC spectra of [^{15}N] eIF3c-A (panel A) and [^{15}N] eIF3c-B (panel B) in the presence of eIF1 at indicated molar ratio. Amino acids assigned by determining the structure of eIF3c-B$_{36\text{-}163}$ are indicated in both the panels. For each panel, close-up views display CSP at resonances highlighted by five thin squares in the spectra with CSP shown by arrows. Black dots indicate the locations of assigned amino acids whose resonances are not affected by eIF1 addition. Red brown dots indicate the locations of amino acids whose resonances displayed line-broadening. Asterisk, unassigned resonance.

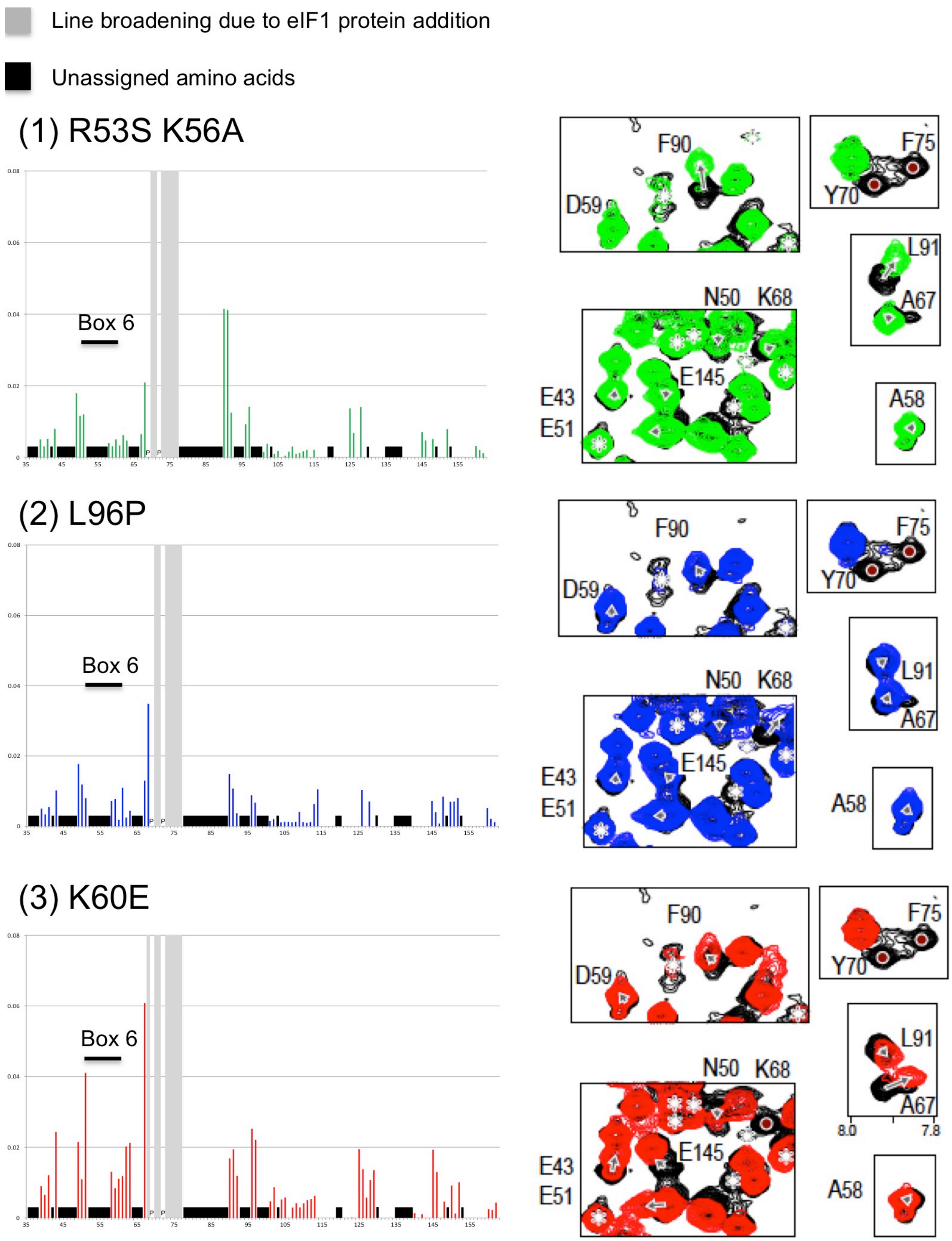

Fig. S4. Chemical shift perturbation observed for eIF3c-B$_{36\text{-}163}$ upon addition of different eIF1 mutants, R53S K56A (panel 1), L96P (panel 2), and K60E (panel 3). – Related to Figure 1

Left, Chemical shift perturbation (CSP), Δδ, was computed as described in Supplementary Materials and methods and presented for each assigned amino acid. "P"s indicate proline residues. Black boxes indicate the residues that were not assigned. Shaded regions indicate the residues whose signal in the ^{1}H-^{15}N HSQC spectra disappeared upon complex formation (line broadening). Right, ^{1}H-^{15}N HSQC spectra of ^{15}N-eIF3c eIF3c-B in the absence (black) or presence of indicated mutant eIF1 protein species (panels 2-4) (1:1.2 in color). For CSP experiment with wild-type eIF1 control, see Fig. 1D and E.

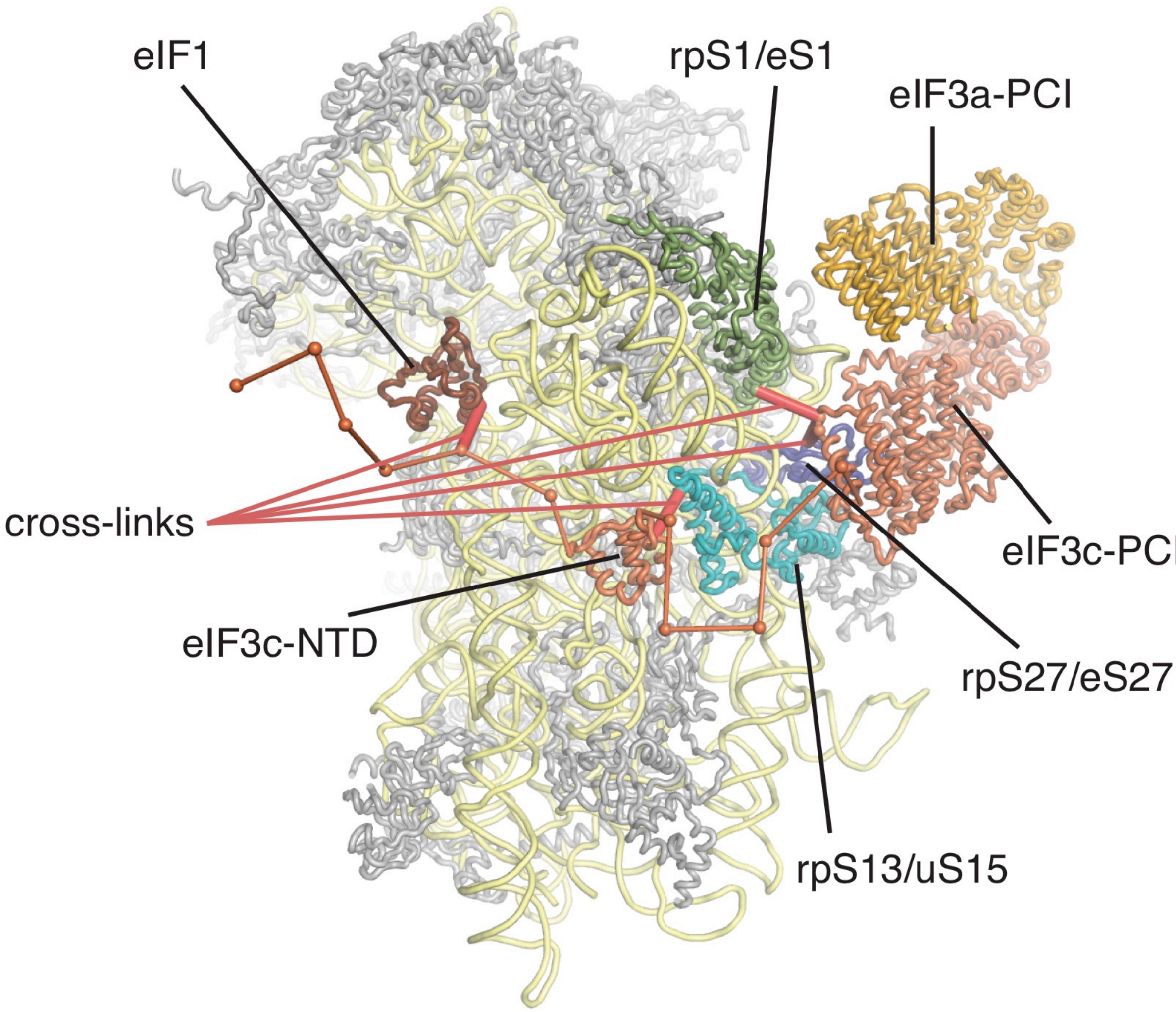

Fig. S5. Representative example of an integrative modeling solution. – Related to Figure 2

Cartoon representation of one of the 500 solutions generated by our modeling runs. eIF3a is colored gold, eIF3c in orange, eIF1 in brown, rpS13/uS15 in cyan, rpS27/eS27 in blue and rpS1/eS1 in green. Interstrand crosslinks are shown in red. Additional structural elements present in the modeling have been omitted for clarity.

A

Sample in Well	Titrant in Syringe	Binding Affinities	
eIF3c-WT (res 1-156)	eIF1-WT (res 1-108; full)	K_d	~ 7 uM
eIF3c-WT (res 1-156)	eIF1-I3N (mutant)	K_d	~ 5 uM
eIF3c-WT (res 1-156)	eIF1-R33A (mutant)	K_d	~ 11 uM
eIF3c-WT (res 1-156)	eIF1-R36E (mutant)	K_d	~ 7.5 uM
eIF3c-WT (res 1-156)	eIF1-K37E (mutant)	K_d	~ 28 uM
eIF3c-WT (res 1-156)	eIF1-K60E (mutant)	K_d	~ 8 uM
eIF3c-WT (res 1-156)	eIF1-L96P (mutant)	K_d	~ 67 uM
eIF3c-WT (res 36-163)	eIF1-WT (res 1-108; full)	K_d	~6.1 uM
eIF3c-WT (res 36-163)	eIF1-R53S (mutant)		Weak
eIF3c-WT (res 36-163)	eIF1-K56A (mutant)	K_d	~ 11 uM
eIF3c-WT (res 36-163)	eIF1-R53S/K56A (mutant)		Weak

B

eIF1 Mutants	40S +eIF1A K_d (nM)	
	Exp I	Exp II
WT	1.6 ± 0.4	10.5 ± 2.0
K60E		>500*
L96P		35 ± 2.0
K56A	17.5 ± 1.9	
R53S	5.6 ± 2.5	
R53S K56A	26.0 ± 4.4	
K37E		> 1000*

Fig. S6. **Additional quantitative interaction assays involving eIF1**. **– Related to Figure 5**

(A) Summary of affinity of various eIF1 mutant proteins for eIF3c-N $_{1\text{-}156}$ (2) or eIF3c-B $_{36\text{-}163}$ (this study), as measured by ITC. Their affinity for WT eIF1 is slightly lower probably due to polyhistidine-tag attached to eIF1. Weak, interaction detected but not quantified due to the curve not fitting to a sigmoid curve. (B) Summary of affinity of eIF1 binding to 40S:eIF1A complex. In Experiment I, wild-type fluorescein-tagged eIF1 was allowed to bind the 40S subunit in the presence of eIF1A and various amounts of indicated eIF1 species, as depicted in Fig. 5B. K_D was computed, based on 3-6 assays. In Experiment II, K_D values were directly measured using the eIF1 variants (WT and mutants) labeled with fluorescein on their C termini. The average of 2 or 3 assays was presented. *, values from a previous study (3).

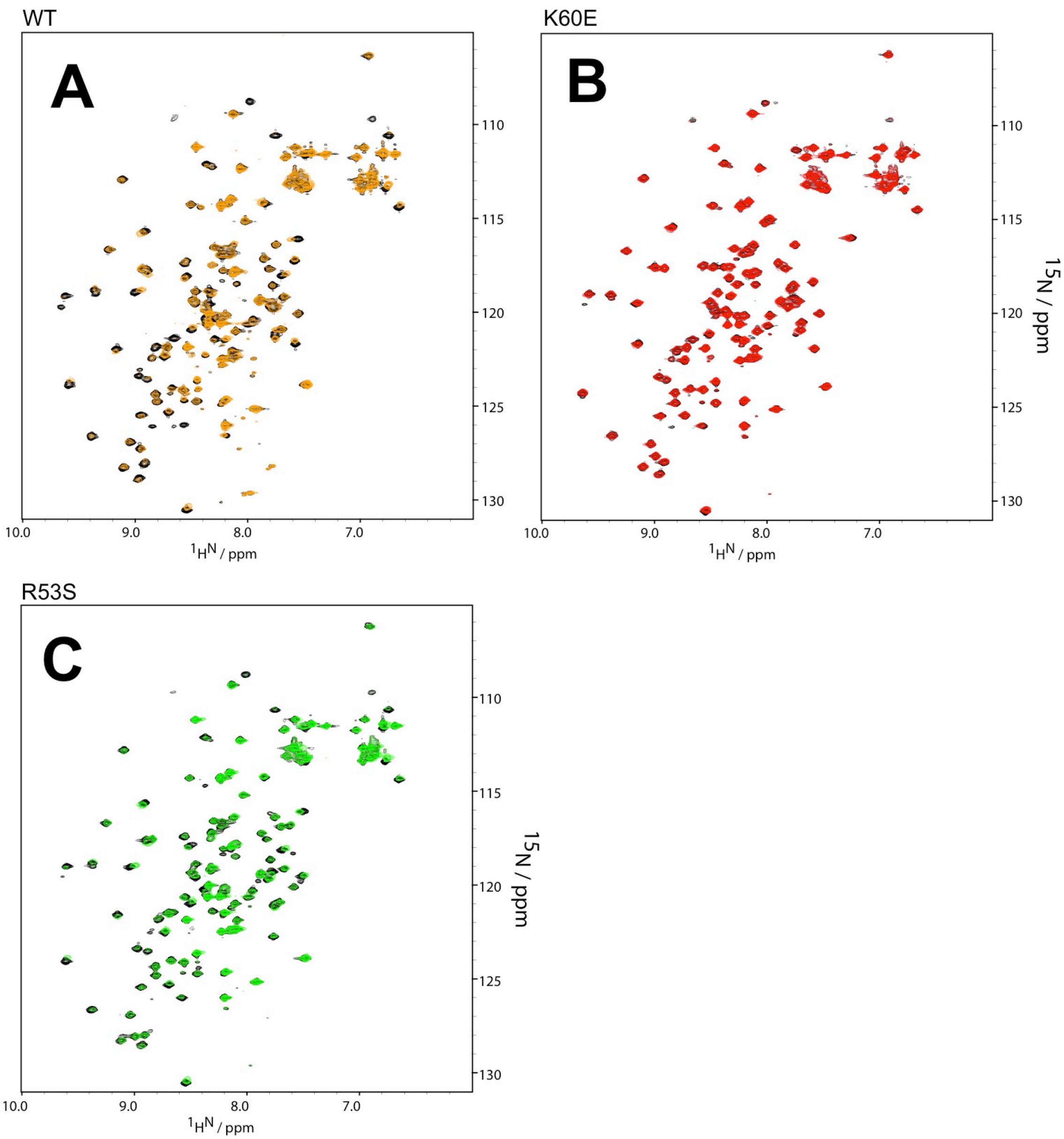

Fig. S7. CSP experiments with WT and mutant ^{15}N-eIF1 and unlabeled eIF5-CTD (aa. 242-405). – Related to Figure 5

(A) HSQC spectra of [^{15}N] WT eIF1 free (gray) or [^{15}N] eIF1: eIF5-CTD = 1 : 4 (orange). (B) HSQC spectra of [^{15}N] eIF1-K60E free (gray) or [^{15}N] eIF1-K60E: eIF5-CTD = 1 : 4 (red). (C) HSQC spectra of [^{15}N] eIF1-R53S free or [^{15}N] eIF1-R53S: eIF5-CTD = 1 : 4 (green).

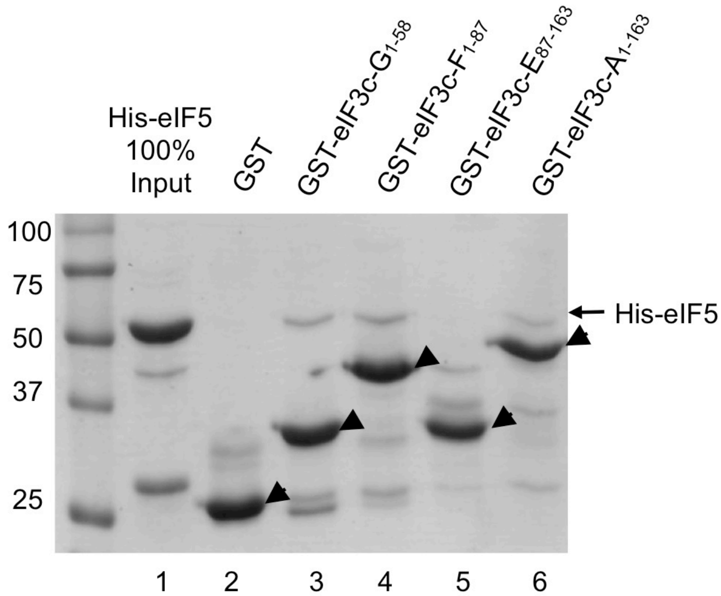

Fig. S8. GST-eIF3c pulldown assays with eIF5. – Related to Figure 8

5 μg of GST or GST-eIF3c fusion proteins listed across top (0.12~0.17 nmol) are allowed to bind 5 μg of His-tagged eIF5 (~0.1 nmol; shown as in-put in lane 1) in a 0.2 ml binding reaction and the complexes were isolated and analyzed by Coomassie staining as in Fig. 3B. Horizontal arrow, the location of His-eIF5. Arrowhead, the location of full-length GST fusion proteins.

Table S1. Plasmids employed in this study – Related to Figures 1, 3, 5, 6, and 7

p #	Systematic name	Description	Source	Used in:
188	pGEX-TIF5-B6	To express GST-eIF5 241-405	(4)	Fig. 5E
596	pGEX-SUI3ΔS	To express GST-eIF2b 1-140	(5)	
283	pGEX-NIP1-N	To express GST-eIF3c 1-156	(2)	
225	pT7-SUI1	To express eIF1 under T7 promoter	(6)	
PMB80	pT7- SUI1-I3N	pT7-SUI1 carrying I3N	This study	
PMB81	pT7- SUI1-K60E	pT7-SUI1 carrying K60E	This study	
PMB82	pT7-SUI1-L96P	pT7-SUI1 carrying L96P	This study	
1157	pET28-His-eIF1	To express His-TEV-eIF1 and purify (untagged) eIF1	This study	Fig. 1, 3, 5 and 7
1490	pET28-His-eIF5 242-405	To express His-eIF5 242-405	This study	Fig. S7
1489	pET28-His-eIF3c 1-163	To express His-eIF3c A 1-163	This study	Fig. 1, 3, 7BC, S2, S3 and S4
1491	pET28-His-eIF3c 1-87	To express His-eIF3c F 1-87	This study	
1492	pET28-His-eIF3c 36-163	To express His-eIF3c B 36-163	This study	
1493	pET28-His-eIF3c 58-163	To express His-eIF3c D 58-163	This study	
1494	pET28-His-eIF3c 87-163	To express His-eIF3c E 87-163	This study	
1507	pET28-His-eIF3c 36-87	To express His-eIF3c C 36-87	This study	
1496	pET28-GST-eIF3c 1-163	To express GST-eIF3c A 1-163	This study	Fig. 1B, 7A, S1BC and S8
1497	pET28-GST-eIF3c 1-87	To express GST-eIF3c F 1-87	This study	
1498	pET28-GST-eIF3c 1-58	To express GST-eIF3c G 1-58	This study	
1499	pET28-GST-eIF3c 36-163	To express GST-eIF3c B 36-163	This study	
1500	pET28-GST-eIF3c 58-163	To express GST-eIF3c D 58-163	This study	
1501	pET28-GST-eIF3c 87-163	To express GST-eIF3c E 87-163	This study	
1505	pET28-GST-eIF3c 36-87	To express GST-eIF3c C 36-87	This study	
1502	pET28-SUI1	To express wild-type eIF1	This study	Fig.1B,5E

				and S1C
1504	pET28-His-eIF5	To express His-eIF5	This study	Fig. 7, S8
1590	pET28-His-eIF1 R53S K56A	To express His-eIF1 R53S K56A	This study	Fig. 5, S6A and S7
1591	pET28-His-eIF1 K60E	To express His-eIF1 K60E	This study	
1594	pET28-His-eIF1 R53S	To express His-eIF1 R53S	This study	
1596	pET28-His-eIF1 L96P	To express His-eIF1 L96P	This study	
1598	pET28-His-eIF1 K56A	To express His-eIF1 K56A	This study	
347	pHis-NIP1-N	To express His-eIF3c 1-156	(2)	Fig. S6A
636	pET-SUI1-His	To express eIF1-His	(7)	
5707	pET-sui1-I3N-His	To express eIF1-I3N-His	(3)	
5708	pET-sui1-K60E-His	To express eIF1- K60E-His	(3)	
5709	pET-sui1-R33A-His	To express eIF1- R33A-His	(3)	
5710	pET-sui1-K37E-His	To express eIF1- K37E-His	(3)	
1595	pET28 eIF1 R53S	To express eIF1 R53S	This study	Fig. 5E
1124	YDpU-SUI3	lc *SUI3 URA3* plasmid	(8)	Fig. 6
1125	YDpU-SUI3-2	lc *SUI3-2 (eIF2β-S264Y) URA3*	(8)	
1647	YCpL-SUI1 K56A	sc *SUI1 LEU2* plasmid carrying *SUI1 K56A*	This study	
1648	YCpL-SUI1 R53S	sc *SUI1 LEU2* plasmid carrying *SUI1 R53S*	This study	
1649	YCpL-SUI1 R53S K56A	sc *SUI1 LEU2* plasmid carrying *SUI1 R53S K56A*	This study	
1789	YDpW-SUI3	lc *SUI3 TRP1* plasmid	This study	
1790	YDpW-SUI3-2	lc *SUI3-2 (eIF2β-S264Y) TRP1*	This study	

Table S2. Yeast *Saccharomyces cerevisiae* strains used in this study – Related to Figure 6

Strain	Genotype	Source
JCY03	*MATa ura3-52 leu2-3 leu2-112 trp1Δ63 his4-301(ACG) sui1Δ::hisG p(sc URA3 SUI1*)	(9)
PMY32	*MATa ura3-52 leu2-3 leu2-112 trp1Δ63 his4-301(ACG) sui1Δ::hisG p(sc LEU2 SUI1-K60E*)	(10)
PMY33	*MATa ura3-52 leu2-3 leu2-112 trp1Δ63 his4-301(ACG) sui1Δ::hisG p(sc LEU2 SUI1-L96P*)	(10)
KAY1057	*MATa ura3-52 leu2-3 leu2-112 trp1Δ63 his4-301(ACG) sui1Δ::hisG p(sc LEU2 SUI1*)	This study
KAY1070	*MATa ura3-52 leu2-3 leu2-112 trp1Δ63 his4-301(ACG) sui1Δ::hisG p(sc LEU2 SUI1-K56A*)	This study
KAY1071	*MATa ura3-52 leu2-3 leu2-112 trp1Δ63 his4-301(ACG) sui1Δ::hisG p(sc LEU2 SUI1-R53S*)	This study
KAY1072	*MATa ura3-52 leu2-3 leu2-112 trp1Δ63 his4-301(ACG) sui1Δ::hisG p(sc LEU2 SUI1-R53S K56A*)	This study

Table S3. Structural Statistics for eIF3c NTD (fragment B, aa. 36-163) – Related to Figure 1

NMR restraints	
Distance restraints	
Total NOE	790
Intra-residue	272
Inter-residue	
Sequential ($\|i - j\| = 1$)	213
Medium-range ($1 < \|i - j\| < 5$)	168
Long-range ($\|i - j\| \geq 5$)	137
Hydrogen bonds restraints [a]	0
Dihedral angle restraints [a]	
φ and ψ	14/14
χ^1 and χ^2	0/0
Structure statistics (20 conformers)	
CYANA target function (Å^2)	0.46
Residual NOE violations	
Number > 0.1 Å	5
Maximum (Å)	0.29
Residual dihedral angle violations	
Number > 5°	0
Maximum (°)	1.85
AMBER energies (kcal/mol)	
Mean AMBER energy	-4730
Mean restraints violation energy	5.34
Ramachandran plot statistics (%) [b]	
Residues in most favored regions	82.3
Residues in additionally allowed regions	15.6
Residues in generously allowed regions	1.6
Residues in disallowed regions	0.5
Average R.M.S.D. to mean structure (Å) [c]	
Protein backbone	0.65 ± 0.20
Protein heavy atoms	1.34 ± 0.26

[a] Used only in CYANA calculations.

[b] Calculated with PROCHECK-NMR.

[c] For residues Asp125-Arg155 of eIF3c 36-163.

Table S4. Structural Statistics for eIF1 – Related to Figure 3

NMR restraints	
Distance restraints	
Total NOE	1560
Intra-residue	463
Inter-residue	
Sequential ($\|i - j\| = 1$)	394
Medium-range ($1 < \|i - j\| < 5$)	261
Long-range ($\|i - j\| \geq 5$)	442
Hydrogen bonds restraints [a]	0
Dihedral angle restraints [a]	
φ and ψ	58/52
χ^1 and χ^2	2/11
Structure statistics (20 conformers)	
CYANA target function (Å^2)	0.19
Residual NOE violations	
Number > 0.1 Å	1
Maximum (Å)	0.23
Residual dihedral angle violations	
Number > 5^o	0
Maximum (^{o})	2.60
AMBER energies (kcal/mol)	
Mean AMBER energy	-3633
Mean restraints violation energy	4.96
Ramachandran plot statistics (%) [b]	
Residues in most favored regions	89.3
Residues in additionally allowed regions	9.8
Residues in generously allowed regions	0.5
Residues in disallowed regions	0.4
Average R.M.S.D. to mean structure (Å) [c]	
Protein backbone	0.48 ± 0.12
Protein heavy atoms	1.10 ± 0.12

[a] Used only in CYANA calculations.

[b] Calculated with PROCHECK-NMR.

[c] For residues Asn24-Ile30, Leu39-Val69, Ile77-Phe108 of eIF1.

Supplemental Results

The effect of eIF1-K60E on eIF1 binding to its MFC partners

The K60E substitution strongly impairs 40S binding in vitro, thereby allowing mis-initiation from UUG codons *in vivo* (Sui^- phenotype) (3). Our GST pulldown assays indicated that K60E also disrupts eIF1 binding to eIF2β-NTT and the eIF5-CTD (Fig. 5E, col. 3); a defect in eIF5-CTD binding was confirmed by CSP assay with ^{15}N-eIF1-K60E (Fig. S7). It is noteworthy that the K60E substitution essentially eliminates eIF1 binding to the 40S subunit (Figs. 5B and S6B) (3) as well as to the eIF2β-NTT and eIF5-CTD (Fig. 5B), and yet, confers a less dramatic increase in UUG initiation compared to L96P (Fig. 6A). One possibility is that eIF1-K60E's robust interaction with eIF3c-NTD (Fig. 5B and E) is sufficient to prevent a more dramatic reduction in accuracy for this substitution *in vivo*. Another possibility in light of the proposed role for 3c0-$Box6_{Ssu+}$ in eIF1 release is that the inability of eIF1-K60 to bind eIF2β-NTT dampened inaccurate UUG initiation by stabilizing the open state, assuming that eIF2β-NTT contributes to eIF1 release by preventing eIF1 rebinding to the ribosome. These two possibilities must be distinguished by experiments in the future.

Supplemental Experimental Procedures

Plasmid construction – Plasmids used in this study are listed in Table S1 and new plasmids were constructed as follows: For protein purification, the genes encoding various yeast *S. cerevisiae* eIF proteins (wild-type or mutant) or their segments were amplified by PCR using budding yeast genomic DNA. The PCR products were digested with BamHI and NotI and then ligated into suitably cut, modified pET28b vector, in which a SD sequence, initial ATG, hexa-histidine tag or GST tag with a tobacco etch virus (TEV) protease cleavage site had been cloned between XbaI and BamHI restriction sites immediately upstream of the protein coding region (pET28-His or pET28-GST derivatives). pET28b derivatives expressing untagged eIF1 or its mutants were also constructed.

For yeast genetics, YCpL-SUI1 (eIF1) derivatives carrying eIF1 R53 and K56 mutations (used in Fig. 6) were constructed by subcloning the 0.2-kb NdeI-BamHI fragment containing the N-terminal half of eIF1-coding region of the corresponding derivatives of pET28-SUI1 plasmids into the same sites of YCpL-SUI1ΔNde (5). YDpW-SUI3 and YDpW-SUI3-2 were constructed by transferring 1.9-kb NotI-SalI fragment of YDpU-SUI3 and YDpU-SUI3-2 (8) into the same sites of pRS414 (lc *TRP1*).

Yeast strains and methods – Yeast strains used in this study are listed in Table S2. Derivatives of strain KAY1057 [*his4-301(ACG) sui1Δ*] were constructed by transforming JCY03 to Leu$^+$ with YCpL-SUI1 (5) or its derivatives carrying the corresponding eIF1 mutations (Table S1), and the resident *SUI1*$^+$ *URA3 plasmid* was evicted by selecting against *URA3* using the drug 5-FOA. Standard yeast molecular biology methods including growth and β-galactosidase assays were used throughout (11).

For UUG initiation assays, we used histidine auxotrophic assay and β-galactosidase assay, using *his4-301(ACG)* allele and *HIS4*^{AUG} or *his4*^{UUG}*-lacZ* fusion plasmids as reporters, respectively. Sui$^-$ mutations allow the *his4-301* allele to express using its third codon, UUG, as the start codon. Thus, yeast *his4-301* strains carrying eIF1 mutant alleles (used in Fig. 6A and listed in Table S2) were assayed for histidine auxotrophy. 5 μl of 1.5 A_{600} units of these strains and their 10-fold serial dilutions are spotted onto synthetic complete (SC) medium lacking leucine (panel 1, +His) or the same medium except with trace histidine (3 μM; panel 2, - His) and incubated for 2 and 10 days, respectively. The growth in the – His plate depends on UUG-initiated translation of a histidine enzyme, and hence a phenotypic measurement of UUG initiation. To quantify UUG initiation frequency compared to AUG initiation, we transformed the eIF1 mutant strains with *URA3 HIS4*^{AUG} and *his4*^{UUG}*-lacZ* fusion plasmids and assayed for β-galactosidase, as described (11).

Likewise, to evaluate the combined effect of eIF1-*R53S* and eIF2β-*S264Y* (in Fig. 6B), overnight cultures of transformants of KAY1057 (WT eIF1) or KAY1071 (eIF1-*R53S*) carrying YDpSUI3 (WT eIF2β) or YDpSUI3-2 (eIF2β-*S264Y*) were spotted similarly onto SC medium lacking uracil (panel 1, +His) or the same medium except with trace histidine (1 μM; panel 2, - His) and incubated for 2 and 9 days, respectively. For *lacZ* reporter assays, we used the KAY1057 and KAY1071 transformants carrying YDpW-SUI3-2 (*SUI3-2 TRP1*) and *URA3 HIS4*^{AUG} or *his4*^{UUG}*-lacZ* fusion plasmids and assayed, as described above.

GST-pulldown assays – GST-pulldown assays were performed as described previously (12). In Fig. 3E, GST-eIF3c-N_{1-156}, GST-eIF2β-NTT_{1-140}, and GST-eIF5-$CTD_{241-405}$ were allowed to bind ^{35}S-labeled eIF1 or its mutant species. The percentage of ^{35}S-eIF1 species pulled down with GST fusion proteins was quantified using a phosphoriager. Alternatively, we used WT and R53S versions of recombinant eIF1 expressed in bacteria for the pulldown assay. In this figure, the values for the binding of each eIF1 mutant are presented relative to those obtained with WT eIF1. Other experiments shown in Fig. 1B, 7A, S1B-C and S8 were done with GST-eIF3c-NTD derivatives and eIF1 and eIF5 that were expressed and purified in *E. coli*. In the case of Fig. 7A, we used an untagged, recombinant form of eIF1 present in *E. coli* lysate, in order to obtain a high concentration required for the competition assay. The amount of eIF1 in the lysate was determined by comparison with known amounts of eIF1 by immunoblotting with anti-eIF1. The same lysate (together with control uninduced lysate) was used for a regular binding assay with eIF1 in Fig. 1B.

Expression and purification of proteins – The pET28-His(TEV) plasmids encoding the desired proteins were employed for transformation of BL21(DE3)RIPL CodonPlus strain (Stratagene). The proteins were expressed in LB medium overnight at 15°C after induction with 0.5 mM IPTG. For His-tagged proteins, harvested cells were re-suspended in Ni-NTA binding buffer (20 mM Tris pH 8.0, 500 mM NaCl, 100 mM urea, 25 mM imidazole and 10 mM β-mercaptoethanol) and lysed using EmulsiFlex homogenizer (Avestin). After centrifugation, the supernatant was loaded onto Ni-NTA agarose (Qiagen) equilibrated with the same buffer. Proteins were eluted by a 25-500 mM linear gradient of imidazole. For GST-tagged proteins, cells were resuspended in GST binding buffer (20mM Tris pH 8.0, 100 mM NaCl and 1 mM DTT) and lysed using EmulsiFlex homogenizer (Avestin). After centrifugation, the supernatant was loaded onto glutathione sepharose (GE) equilibrated with the same buffer. Proteins were eluted by a 0-10 mM linear gradient of reduced glutathione. Peak fractions were incubated overnight with His-tagged TEV protease at room temperature while dialyzing against Ni-NTA low salt buffer (20 mM Tris pH 8.0, 100 mM NaCl, 25 mM imidazole and 10 mM β-mercaptoethanol). After complete cleavage the sample was loaded on Ni-NTA agarose again to remove His tag, His-tagged TEV protease and minor protein contaminants. The complex was then dialyzed against the buffer (20 mM Tris pH 8.0, 100 mM NaCl) for the measurements.

ITC experiments – All calorimetric titrations were carried out on VP-ITC and iTC200 calorimeters (MicroCal). Protein samples were dialyzed against the buffer containing 25 mM Tris pH 8.0 and 100 mM NaCl. The sample cell was filled with 50 μM solution of eIF1 and the injection syringe with 500 μM of the titrating eIF3c. For VP-ITC, each titration typically consisted of a preliminary 3 μl injection followed by 28 subsequent 10 μl injections every 210 seconds. For iTC200, each titration typically consisted of a preliminary 0.4 μl injection followed by 19 subsequent 2 μl injections every 150 seconds. All of the experiments were performed at 20°C. Data for the preliminary injection, which are affected by diffusion of the solution from and into the injection syringe during the initial equilibration period, were discarded. The data were fitted using ORIGIN software.

NMR spectroscopy – For structural determinations, [^{13}C, ^{15}N] eIF1 and [^{13}C, ^{15}N] eIF3c-B_{36-163} were each concentrated to 0.4 mM in 20 mM sodium phosphate buffer (pH 7.0), containing 150 mM NaCl and 1 mM 1,4-DL-dithiothreitol (DTT), using Amicon Ultra15 filter (3000 MWCO, Millipore). In this study, we used an untagged, native form of eIF1 by a TEV-protease cleavage method, determined its structure and used it for interaction mapping studies. All NMR data were collected at 298 K on Bruker AVANCE III HD 600, Bruker AVANCE 600 and 800 MHz NMR spectrometers, each equipped with a cryogenic probe. NMR spectra were processed with NMRPipe/NMRDraw (13). Spectral analysis was performed with KUJIRA 0.984 (14), a program suite for interactive NMR analysis working with NMRView (15), according to the methods described previously (16). The backbone and side chain ^{1}H, ^{15}N and ^{13}C resonances of the proteins were assigned by standard double- and triple-resonance NMR experiments (17, 18), and were deposited in the BioMagResDB (BMRB accession numbers 11599 for eIF1 and 11600 for eIF3c-B). Distance restraints were derived from three-dimensional (3D) ^{15}N-edited and ^{13}C-edited nuclear Overhauser effect spectroscopy (NOESY)-HSQC spectra, each measured with a mixing time of 80 ms.

Structure calculations – Structure calculations of eIF1 and eIF3c-B $_{36\text{-}163}$ were performed using CYANA 2.0.17 (19-21). The structure calculations started from 200 randomized conformers, and used the standard CYANA simulated annealing schedule with 40,000 torsion angle dynamics steps per conformer. The 40 conformers with the lowest final CYANA target function values were further refined with AMBER9 (22), using the AMBER 2003 force field and a generalized Born model, as described previously (16). The 20 conformers that were most consistent with the experimental restraints were then used for further analyses. The final structures were validated and visualized by using the PROCHECK-NMR (23) and CHIMERA (24, 25). Detailed experimental data and structural statistics are summarized in Table S3 and S4. The final ensembles of 20 conformers were deposited in the Protein Data Bank (PDB IDs 2rvh for eIF1 and 5H7U for eIF3c-B).

Chemical shift perturbation experiments – All the proteins were dissolved in 20 mM sodium phosphate buffer (pH 7.0), containing 150 mM NaCl and 1 mM DTT. A series of 2D ^{1}H–^{15}N HSQC spectra were recorded for the samples containing 70 μM [^{15}N] eIF3c-A $_{1\text{-}163}$ or [^{15}N] eIF3c-B $_{36\text{-}163}$ and unlabeled eIF1 at the molar ratios of 1.0:0.0, 1.0:0.3, 1.0:0.6, and 1.0:1.0. The samples containing 70 μM [^{15}N] eIF3c-B $_{36\text{-}163}$ and either eIF1-K60E, eIF1-L96P, or eIF1-R53S/K65A at the molar ratios of 1.0:0.0 and 1.0:1.2; and the samples containing 70 μM of either [^{15}N] eIF1, or [^{15}N] eIF1-K60E, [^{15}N] eIF1-R53S and eIF5$_{242\text{-}405}$ at the molar ratios of 1.0:0.0 and 1.0:4.0 were also subjected to 2D ^{1}H–^{15}N HSQC spectra measurements. These spectra were processed with NMRPipe/NMRDraw[1] and analyzed with Sparky (26). Chemical shift perturbation (CSP), Δδ, was defined as $\Delta\delta = [(\Delta\delta_H)^2+(\Delta\delta_N/6.5)^2]^{1/2}$, where $\Delta\delta_H$ and $\Delta\delta_N$ are the chemical shift differences for H^N and ^{15}N, respectively, and 6.5 is the scaling factor determined from the ratio of the average variances of the H^N and ^{15}N chemical shifts observed for the 20 common amino acid residues in proteins (27).

To verify the assignment of perturbed amino acids, we used [^{13}C, ^{15}N] eIF3c-C $_{36\text{-}87}$ and re-assigned amino acids in the presence of eIF1. This helped us verify the perturbation of ~ 10 overlapping chemical shifts. In the ^{15}N-eIF1 CSP experiments with eIF5-CTD, we also used eIF5 $_{242\text{-}396}$ lacking the C-terminal tail. The CSP observed with this segment was indistinguishable with that observed with eIF5 $_{242\text{-}405}$ (Fig. 1E, left), indicating that eIF5-CTD, not the C-terminal tail, interacts with eIF1.

Fluorescence Anisotropy Experiments – Initiation factors eIF1A and eIF1 WT and mutant variants of this protein were purified using the IMPACT system (New England Biolabs) as described before (28) using the appropriate pTYB2-derived constructs. eIF1 WT and mutant proteins were labeled at their C termini with cysteine-lysine-fluorescein dipeptide, using the expressed protein ligation system as described previously (29). 40S subunits were purified as described previously (28).

Fluorescence anisotropy measurements of equilibrium binding constants (*Kd*) were performed using a T-format Spex Fluorolog-3 (J. Y. Horiba) as described previously (29). The excitation and emission wavelengths were 497 and 520 nm, respectively.

The data were fit with a hyperbolic binding equation describing the binding of fluorescently labeled eIF1 mutants to 40S subunits to give *Kd* values (29). In competition experiments with unlabeled eIF1, the data were fit with a quadratic equation describing the competitive binding of two ligands to a receptor (29).

Analytical ultracentrifugation (AUC) – AUC sedimentation velocity experiments were carried out in the AUC buffer (20 mM sodium phosphate, pH 7.0, 150 mM NaCl), using an Optima XL-I analytical ultracentrifuge equipped with two optical systems, the Rayleigh interference and absorbance systems (Beckman Coulter). For centrifuge, we used an An-50 Ti rotor featuring cells with a standard 12-mm charcoal-epon double sector centerpiece and sapphire windows. Proteins were diluted with the AUC buffer to a final concentration of 20-25 uM each. After dialysis with the same buffer, the sample was loaded into a cell in the An-50 Ti rotor. The experiments were conducted at 50,000 rpm at a temperature of 293 K. During the runs, changes in the protein concentration gradient were monitored with absorbance at 280 nm. All of raw data were analyzed by the program SEDFIT14.1, with the continuous C(s) distribution model (30). The SEPHAT 10.58d program was used for analysis of the isotherm of weight-average s-values.

Supplemental References

1. Martin-Marcos P*, et al.* (2013) β-hairpin loop of eIF1 mediates 40S ribosome binding to regulate initiator tRNAMet recruitment and accuracy of AUG selection in vivo. *J Biol Chem* 288:27546-27562.
2. Singh CR, Hui H, Ii M, Yamamoto Y, & Asano K (2004) Efficient incorporation of eIF1 into the multifactor complex is critical for formation of functional ribosomal preinitiation complexes in vivo. *Journal of Biological Chemistry* 279:31910-31920.
3. Watanabe R*, et al.* (2010) The eIF4G HEAT domain promotes translation re-initiation in yeast both dependent on and independent of eIF4A mRNA helicase. *J Biol Chem* 285:21922-21933.
4. Lee B, Udagawa T, Singh CS, & Asano K (2007) Yeast phenotypic assays on translational control. *Methods Enzymol* 429:139-161.
5. Singh CR & Asano K (2007) Localization and characterization of protein-protein interaction sites. *Methods Enzymol* 429:139-161.
6. Delaglio F*, et al.* (1995) NMRPipe: a multidimensional spectral processing system based on UNIX pipes. *J Biomol NMR* 6:277-293.
7. Kobayashi N*, et al.* (2007) KUJIRA, a package of integrated modules for systematic and interactive analysis of NMR data directed to high-throughput NMR structure studies. *J Biomol NMR* 39:31-52.
8. Johnson BA (2004) Using NMRView to visualize and analyze the NMR spectra of macromolecules. *Methods Mol Biol* 278:313-352.
9. Nagata T*, et al.* (2008) The RRM domain of poly(A)-specific ribonuclease has a noncanonical binding site for mRNA cap analog recognition. *Nucl Acids Res* 36:4754-4767.
10. Clore GM & Gronenborn AM (1998) Determining the structures of large proteins and protein complexes by NMR. *Trends Biotechnol* 16:22-34.
11. Cavanagh J, Fairbrother WJ, Palmer A, G, 3rd, & Skelton NJ (1996) *Protein NMR spectroscopy, principles and practice* (Academic Press, Inc., San Diego, CA).
12. Herrmann T, Güntert P, & Wüthrich K (2002) Protein NMR structure determination with automated NOE assignment using the new software CANDID and the torsion angle dynamics algorithm DYANA. *J Mol Biol* 319:209-227.
13. Guntert P, Mumenthaler C, & Wuthrich K (1997) Torsion angle dynamics for NMR structure calculation with the new program DYANA. *J. Mol. Biol.* 273(1):283-298.
14. Guntert P (2009) Automated structure determination from NMR spectra. *Eur. Biophys. J.* 38(2):129-143.

15. Case DA*, et al.* (2005) The Amber biomolecular simulation programs. *J Comput Chem* 26:1668-1688.

16. Laskowski RA, Rullmann JA, MacArthur MW, Kaptein R, & Thornton JM (1996) AQUA and PROCHECK-NMR: programs for checking the quality of protein structures solved by NMR. *J Biomol NMR* 8:477–486.

17. Meng EC, Pettersen EF, Couch GS, Huang CC, & Ferrin TE (2006) Tools for integrated sequence-structure analysis with UCSF Chimera. *BMC Bioinformatics* 7:339.

18. Pettersen EF*, et al.* (2004) UCSF Chimera--a visualization system for exploratory research and analysis. *J Comput Chem* 25(13):1605-1612.

19. Goddard TD & Kneller DG (2006) *SPARKY 3* (University of California, San Francisco).

20. Mulder FA, Schipper D, Bott R, & Boelens R (1999) Altered flexibility in the substrate-binding site of related native and engineered high-alkaline Bacillus subtilisins. *J. Mol. Biol.* 292(1):111-123.

21. Acker MG, Kolitz SE, Mitchell SF, Nanda JS, & Lorsch JR (2007) Reconstitution of yeast translation initiation. *Methods Enzymol* 430:111-145.

22. Maag D & Lorsch JR (2003) Communication between eukaryotic translation initiation factors 1 and 1A on the yeast small ribosomal subunit. *Journal of Molecular Biology* 330:917-924.

23. Schuck P (2000) Size-distribution analysis of macromolecules by sedimentation velocity ultracentrifugation and lamm equation modelling. *Biophys. J* 78:1606-1619.

24. Edgar RC (2004) MUSCLE: multiple sequence alignment with high accuracy and high throughput. *Nucl Acids Res* 32:1792-1797.

25. Asano K, Clayton J, Shalev A, & Hinnebusch AG (2000) A multifactor complex of eukaryotic initiation factors eIF1, eIF2, eIF3, eIF5, and initiator $tRNA^{Met}$ is an important translation initiation intermediate in vivo. *Genes Dev* 14:2534-2546.

26. Asano K, Krishnamoorthy T, Phan L, Pavitt GD, & Hinnebusch AG (1999) Conserved bipartite motifs in yeast eIF5 and eIF2Be, GTPase-activating and GDP-GTP exchange factors in translation initiation, mediate binding to their common substrate eIF2. *EMBO J* 18:1673-1688.

27. Asano K, Phan L, Anderson J, & Hinnebusch AG (1998) Complex formation by all five homologues of mammalian translation initiation factor 3 subunits from yeast *Saccharomyces cerevisiae*. *J Biol Chem* 273:18573-18585.

28. Reibarkh M*, et al.* (2008) Eukaryotic initiation factor (eIF) 1 carries two distinct eIF5-binding faces important for multifactor assembly and AUG selection *J Biol Chem* 283:1094-1103.

29. Cheung Y-N*, et al.* (2007) Dissociation of eIF1 from the 40S ribosomal subunit is a key step in start codon selection in vivo. *Genes Dev* 21:1217-1230.

30. Martin-Marcos P, Cheung Y-N, & Hinnebusch AG (2011) Functional Elements in Initiation Factors 1, 1A, and 2β Discriminate against Poor AUG Context and Non-AUG Start Codons. *Mol Cell Biol* 31:4814-4831.